ACS ES&T Air

pubs.acs.org/estair

Article

Secondary Organic Aerosol from OH Oxidation of Acyclic Terpenes Is More Viscous and Less Volatile than That of Their Cyclic Analogs

Sijia Liu, Claire E. Moffett, Gregory Vandergrift, Manish Shrivastava, Zezhen Cheng, Swarup China, Sergey A. Nizkorodov, Alla Zelenyuk, and Celia L. Faiola*

Cite This: ACS EST Air 2026, 3, 83−94

Read Online

ACCESS | Metrics & More | Article Recommendations | Supporting Information

ABSTRACT: Biogenic volatile organic compounds (BVOCs), a dominant source of secondary organic aerosol (SOA) globally, exhibit emission rates and compositions that are plant species-specific and vary with environmental stressors. A common outcome of plant stress is increased emissions of acyclic terpenes. The paucity of information about acyclic terpene SOA chemistry contributes to uncertainties in predictions of SOA global loadings and impacts on Earth's radiative budget, particularly in a changing climate where acyclic terpene emissions could become more prominent. This study compared properties of SOA derived from hydroxyl radical (OH) oxidation of acyclic and cyclic monoterpenes (β-ocimene, α-pinene) and sesquiterpenes (β-farnesene, β-caryophyllene). Single-particle mass spectrometry was used for assessing shape, density, and evaporation kinetics of size-selected SOA particles, and nanospray desorption electrospray ionization high-resolution mass spectrometry (nano-DESI-HRMS) was used to measure the molecular composition of SOA. Acyclic terpene SOA exhibited higher viscosity and lower volatility compared to cyclic terpene SOA, and had a greater volume fraction remaining (VFR) after ∼24 h of evaporation—approximately 1.3−1.6 times higher VFR than that of cyclic terpene SOA. Additionally, HRMS analysis revealed greater chemical diversity and higher fractions of extremely low-volatility compounds (56−62% ELVOC/LVOC) in acyclic terpene SOA compared to cyclic counterparts (25−37% ELVOC/LVOC). Our findings highlight the potential importance of accounting for acyclic terpene aerosol chemistry under conditions of plant stress to improve predictions of SOA loadings and impacts.

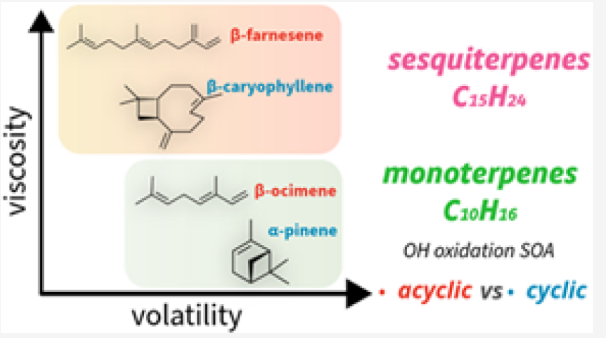

KEYWORDS: *secondary organic aerosol, SOA physical properties, sesquiterpenes, monoterpenes, viscosity, volatility, atmospheric chemistry*

INTRODUCTION

Secondary organic aerosol (SOA) forms in the atmosphere via oxidation of volatile organic compounds (VOCs), influencing cloud formation, earth's radiative balance, and human health.[1−3] SOA viscosity and volatility are important properties that alter particle evaporation and growth kinetics,[4,5] which subsequently influence SOA mass loadings, atmospheric lifetimes, and the cloud condensation nuclei (CCN) budget. Additionally, these properties play important roles in ice nucleation,[6] and atmospheric photochemistry,[7] which are essential processes for predicting SOA loadings and radiative impacts. A substantial source of SOA arises from the oxidation of biogenic volatile organic compounds (BVOCs), such as isoprene, monoterpenes, and sesquiterpenes, which are secondary metabolites emitted from plants.[8−10] These BVOCs play critical ecological functions, providing plant chemical defenses from insect herbivores and pathogens, and facilitating intraspecies and interspecies plant communication.[11−13] The BVOC emission profiles of plants are species-specific and are modulated by environmental context, including plant stress.[14−16] Plants are increasingly subjected to more frequent and severe stress conditions as climate rapidly changes,[17] including, but not limited to, weather extremes, insect outbreaks, and drought, thus influencing plants' BVOC emission rates and composition.[14,16,18−21]

One common plant stress response is elevated emissions of acyclic terpenes, especially acyclic sesquiterpenes, such as farnesene isomers.[22−25] Despite their typical lower ambient concentrations compared to cyclic terpenes, the high reactivity of acyclic terpenes may enhance their role in atmospheric processes beyond what their abundance alone would suggest.[26] For example, the rate coefficient for the reaction of β-ocimene with OH radicals is ∼ 4−5 times higher than that of α-pinene.[27−29] In addition, Jardine et al. found that, despite the lower abundance of ocimene relative to α-pinene in the

Received: June 19, 2025
Revised: December 15, 2025
Accepted: December 16, 2025
Published: December 29, 2025

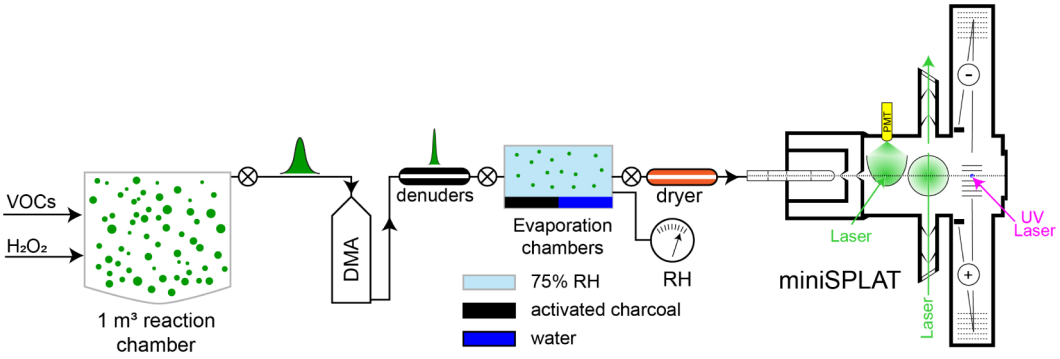

Figure 1. Schematic of the experimental setup for miniSPLAT measurements of evaporation kinetics. SOA from the reaction chamber were size-selected by a differential mobility analyzer (DMA), and then introduced into two evaporation chambers, where particle size distributions and evaporation kinetics were measured periodically by miniSPLAT over approximately 24 h.

Amazon, its cumulative ozonolysis potential was approximately twice as high.[26] There is also mounting evidence that acyclic terpene SOA chemistry is substantially different from that of their cyclic analogs, and depending on the oxidant, may lead to significant differences in physical properties of the resulting SOA. For example, oxidation of acyclic terpenes by ozone has been associated with reduced SOA formation potential compared to cyclic terpene analogs.[24,30−32] The suppression of SOA mass yields during ozonolysis of acyclic terpenes was attributed to an increased level of fragmentation products compared to ozonolysis of bicyclic (e.g., pinenes) and monocyclic (e.g., limonene, phellandrenes) molecular structures.[30−32] In seeming contrast to ozonolysis products, SOA generated by OH-initiated oxidation of VOC mixtures was found to have higher viscosity and increased propensity for liquid−liquid phase separation when the starting VOC mixtures contained more acyclic terpenes.[33−35] Studies of acyclic terpene SOA chemistry are limited compared to their cyclic analogs and significant knowledge gaps remain, particularly with regard to systematic, comparative studies of the composition and physicochemical properties of SOA formed from cyclic versus acyclic terpene precursors.

The current study endeavors to bridge the knowledge gap in understanding the chemical composition, viscosity, and volatility of acyclic terpene SOA by comparing SOA properties from OH photooxidation of both cyclic and acyclic terpenes for two different compound classes − monoterpenes ($C_{10}H_{16}$) and sesquiterpenes ($C_{15}H_{24}$). The four terpenes used in this study were chosen for their prominent contribution to previously reported biogenic emission rates and to include representative compounds for both cyclic (α-pinene, β-caryophyllene) and acyclic (β-ocimene, β-farnesene) structures within the monoterpene and sesquiterpene classes.[26,30,31,36,37] To compare the viscosity and volatility of SOA from cyclic/acyclic and monoterpene/sesquiterpene chemical systems, we utilized miniSPLAT, a single particle mass spectrometer capable of measuring the changes in particle size on the order of a monolayer with extremely high sensitivity and temporal resolution, facilitating the characterization evaporation kinetics and shape of SOA particles during evaporation.[38−40] Nanospray desorption electrospray ionization high resolution mass spectrometry (nano-DESI HRMS) was utilized to examine the initial SOA molecular composition prior to evaporation. Through the integration of state-of-the-art measurements, this study offers new insights into the influence of precursor structure on SOA properties under OH-initiated oxidation. To the best of our knowledge, the current research is the first to systematically compare differences in composition and physical properties across cyclic and acyclic terpene SOA. These results can be used to refine the treatment of biogenic precursors in current regional and global models, particularly under stress-driven emission scenarios involving enhanced acyclic terpene release, and thereby inform continual model development with the aim of improving our understanding of how changing BVOC profiles influence atmospheric processes on a larger scale.

MATERIALS AND METHODS

SOA Generation. SOA was generated in a cube-shaped 1 m^3 fluorinated ethylene propylene (FEP) reaction chamber via OH photooxidation operated in batch-mode. To ensure the absence of residual particulate matter, the reaction chamber was flushed with nitrogen three times, followed by prefilling with zero air prior to each experiment. Subsequently, the VOC was introduced into the particle-free reaction chamber by injecting microliter quantities of α-pinene (Sigma-Aldrich, purity 98%), β-ocimene (Sigma-Aldrich, purity >90%, Lot # SHBL2427), β-caryophyllene (Sigma-Aldrich, purity >98%, Lot # BCBP1878 V), or β-farnesene (Supelco, purity >90%, Lot # BCCD9598) into a round-bottom flask. The flask was gradually heated to 75 °C while being flushed with 10 L/min of zero air to facilitate VOC evaporation into the chamber. Following the VOC injection, the OH radical precursor, 50 wt % hydrogen peroxide, was similarly injected into the 10 L/min air flow via the heated round-bottom flask and transported to the chamber. After introducing all the experiment components, additional clean air was added to the chamber until it reached its final volume of ∼ 1 m^3. VOC photooxidation was initiated by turning on UV−B lights to start the photolysis of H_2O_2 and OH radical generation. All experiments were conducted under dry conditions, low nitrogen oxides (NO_x) and at room temperature (24 ± 1 °C). The detailed experimental conditions and additional description are provided in the Supporting Information (SI, Table S1). Aerosol formation and growth were continuously monitored with a scanning mobility particle sizer (SMPS, TSI, Model 3082). After ∼ 2 h, the UV−B lights were turned off, particles were sampled *in situ* with miniSPLAT, and then all the residual SOA particles in the reaction chamber were collected on Teflon filters (Fluoropore, 0.2 μm PTFE membrane) at 20 L/min for subsequent offline composition analysis via nano-DESI HRMS, using methods developed and validated in previous studies[33−35,41]

https://doi.org/10.1021/acsestair.5c00226
ACS EST Air 2026, 3, 83−94

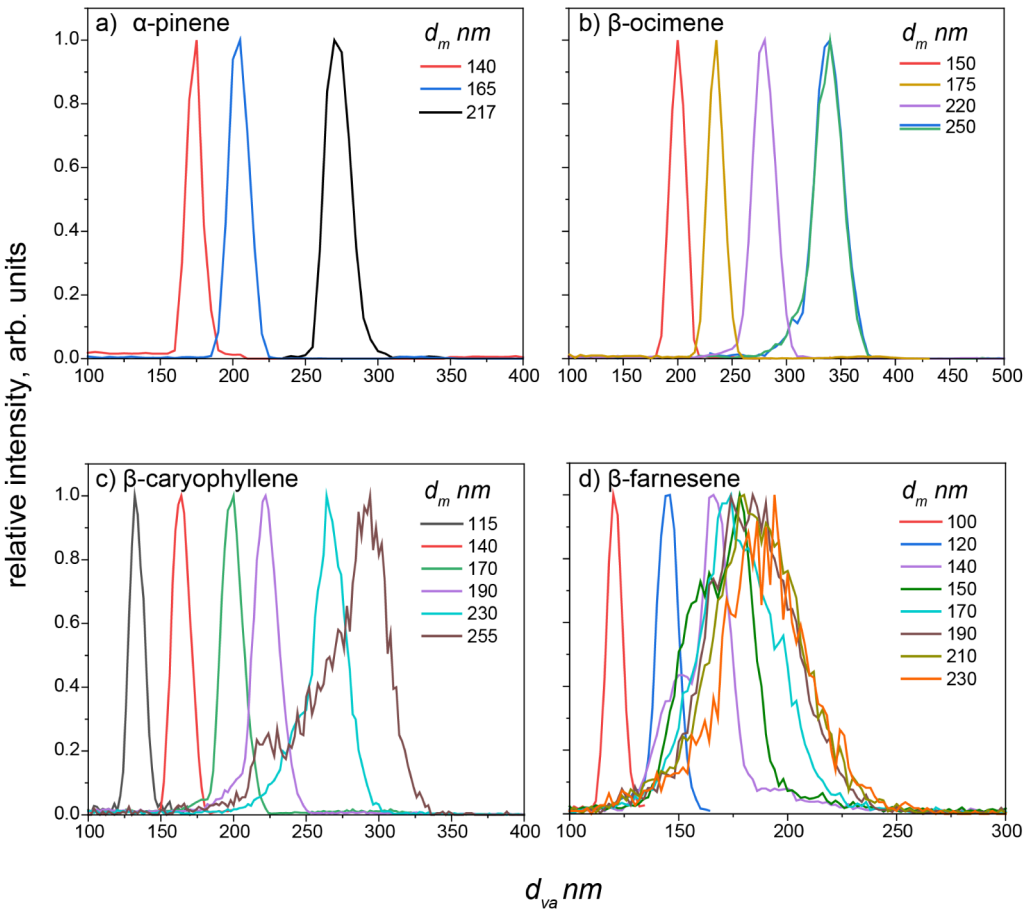

Figure 2. Vacuum aerodynamic diameter (d_{va}) distributions from miniSPLAT for DMA size-selected particles of (a) α-pinene, (b) β-ocimene (250 nm was measured twice to verify the reproducibility of line-shape of d_{va} size distributions), (c) β-caryophyllene, and (d) β-farnesene OH oxidation SOA. The legend corresponding the mobility diameter (d_m) for DMA-selected particles. The narrow distribution widths indicate that the particles are spherical in shape.

miniSPLAT Measurements. Following the formation of SOA, particle vacuum aerodynamic diameter distribution (d_{va}), mass spectra, density, and shape were characterized using methods previously described in detail elsewhere.[38,40] A differential mobility analyzer (DMA, TSI, model 3080) was employed to select monodisperse particles, typically with mobility diameters between 100 and 250 nm, and these particles were sampled by miniSPLAT (Figure S1).[4,42] For each SOA chemical system, particle density and shape were evaluated across a range of particle sizes. For spherical particles, particle density (ρ_p) was quantified from the relationship between measured d_{va} (from miniSPLAT) and mobility diameter (d_m, from DMA), given by the equation $\rho_p = \frac{d_{va}}{d_m}\rho_0$, where ρ_0 stands for unit density (1 g/cm^3). For aspherical particles the same equation yields particle effective density. Particle shape was characterized by examining the width of the d_{va} distribution, wherein a narrow symmetric distribution corresponds to spherical particles and a broader, often asymmetric, distribution indicates the presence of aspherical particles.[5,39]

SOA volatility was determined from particle evaporation kinetics under dry and humid conditions by transferring monodisperse particles (at # concentrations of ∼ 100−200 particles/cm^3) from the SOA generation chamber through the inline denuder used to remove gas-phase organics into two stainless steel evaporation chambers at a flow rate of 0.3 L/min (Figure 1); one evaporation chamber was maintained at dry conditions and was partially filled with activated charcoal to continually strip the gas phase species, and the other evaporation chamber was maintained at 75% RH. Both evaporation chambers were kept at atmospheric pressure and room temperature. This was repeated for each of the acyclic and cyclic terpene SOA systems included in the study. The evaporation process was monitored in both wet and dry evaporation chambers over a ∼ 24 h window by periodically connecting the evaporation chambers to the miniSPLAT and measuring the particles' d_{va} and mass spectra. During the initial stage of evaporation, samples were taken approximately every 30 min to 1 h, followed by one to two additional measurements overnight, per established methods.[4,42] The evaporation kinetics data were fitted using a 7-bin volatility basis set (VBS), with the detailed fitting method described in the SI.[4,42,43]

High-Resolution Mass Spectrometer Measurements. After the evaporation chambers were loaded with particles with desired mobility diameters, the remaining SOA in the reaction chamber was collected on a Teflon substrate (PTFE, 47 mm, Millipore) and immediately frozen at −20 °C. Samples were stored for no longer than 7 days under these conditions, minimizing chemical changes prior to analysis.[44] The SOA filter samples were directly ionized from the filter *in situ* via a nano-DESI source, which was interfaced with a LTQ Velos

https://doi.org/10.1021/acsestair.5c00226
ACS EST Air 2026, 3, 83−94

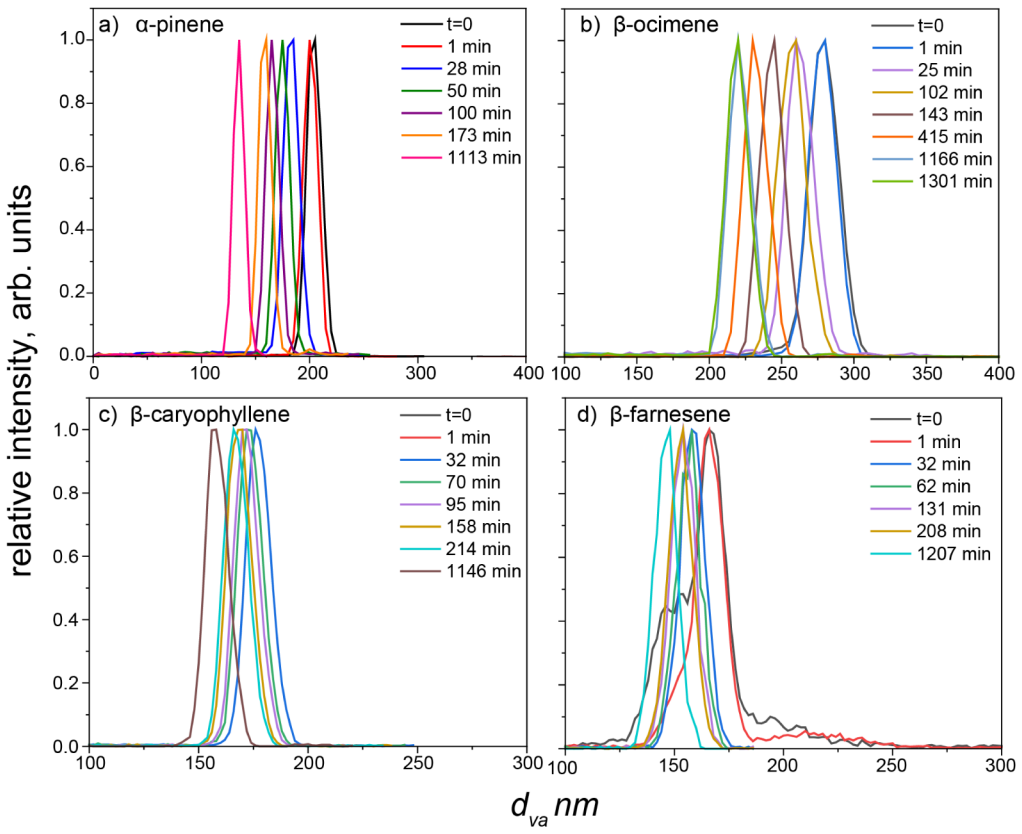

Figure 3. d_{va} distributions of mobility size-selected particles during evaporation under dry evaporation condition (RH < 10%) for: a) α-pinene SOA (d_m = 165 nm), b) β-ocimene SOA (d_m = 220 nm), c) β-caryophyllene SOA (d_m = 165 nm), and d) β-farnesene (d_m = 140 nm).

Orbitrap high resolution mass spectrometer (Thermo Scientific, Waltham).[45,46] The instrument was operated in negative ion mode over a m/z range of 100−1000. The data were extracted using FreeStyle 1.6 and the neutral molecular formula assigned by MFAssignR,[47] as detailed in the SI.

Volatility and Viscosity Prediction. The volatility and viscosity of SOA were predicted from the distribution of observed molecular formulas assigned from the HRMS data using established analytical procedures obtained from Li et al. and DeRieux et al.[48,49] The detailed parameters and equations used are described in detail in the SI.

RESULTS AND DISCUSSION

Particle Shape and Density. Physical properties of the particles formed in the reaction chamber were evaluated before the evaporation experiments were conducted. Particle shape and density can be characterized from miniSPLAT size-selected particle measurements by comparing the mobility and vacuum aerodynamic diameters as shown in Figure 2 where the different colored lines correspond to different sizes of particles selected with the DMA for the evaporation chamber and the x-axis indicates the vacuum aerodynamic diameter of the particles in the evaporation chamber measured with the miniSPLAT. Particle shape is qualitatively characterized based on the width and symmetry of the peak. where narrow distributions and symmetrical peak widths indicate more spherical particles. Particle density is calculated with the equation provided in the methods section, "miniSPLAT measurements." This analysis revealed notable differences among the different SOA types (Figure 2). DMA-selected α-pinene SOA particles with a starting d_m of 165 nm displayed a d_{va} distribution peak at 205 nm, with a narrow line width and symmetrical peak shape indicative of a spherical shape (the blue line on Figure 2a). The 1.24 ± 0.01 g/cm^3 density of α-pinene SOA derived from the measured d_m and d_{va} values is consistent with previous measurements, which range from 1.20 to 1.23 g/cm.[3,50,51] Similar properties were observed for smaller (<250 nm d_m) size-selected β-ocimene SOA particles, yielding particle density of 1.35 ± 0.01 g/cm^3. Note, however, that the d_{va} size distributions of size-selected β-ocimene SOA particles with d_m of 250 nm exhibit a small but reproducible "tail" at smaller $d_{va,}$ indicating the additional presence of a small fraction of aspherical particles, most likely formed by coagulation of smaller SOA particles, similar to previously published observations.[52]

The d_{va} distributions for sesquiterpene SOA particles were narrow for smaller particles, but broader, and asymmetric for larger particles. Figure 2c shows the d_{va} distributions for size-selected β-caryophyllene SOA particles. Particles with smaller d_m (<∼200 nm) exhibit d_{va} distributions that are relatively narrow and symmetric, while particles with larger d_m have broader and more asymmetric distributions, indicating a shift from spherical to a mixture of spherical and aspherical particles with increasing d_m. The presence of aspherical particles was observed for both sesquiterpene SOA, but it was more pronounced for β-farnesene compared to β-caryophyllene. In the case of β-farnesene SOA (Figure 2d), particles with d_m larger than 120 nm display broad distributions with a particularly broad distribution for particles with d_m greater than 190 nm, indicating a substantial fraction of aspherical particles. Larger particles form in the reaction chamber through the coagulation of smaller particles (Figure S2), and

https://doi.org/10.1021/acsestair.5c00226
ACS EST Air 2026, 3, 83−94

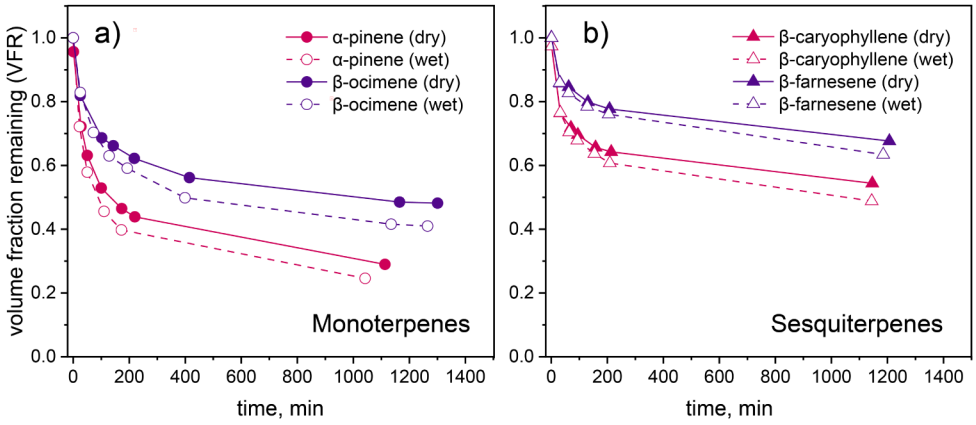

Figure 4. Evaporation kinetics of size-selected SOA particles generated from four different terpene structures. Panel a) shows evaporation behavior of α-pinene and β-ocimene SOA, while panel b) presents β-caryophyllene and β-farnesene SOA. Solid lines represent dry conditions (<10% RH), and dashed lines represent humid conditions (75% RH). Acyclic terpene traces are represented with purple, while cyclic terpene traces are represented with red.

when particle viscosity increases, the coalescence relaxation time needed to the overcome surface tension after the collision and form spherical shapes becomes longer than the experimental time scale, leading to this size-dependent particle shape.[52−55] Therefore, the evidence for increased aspherical particles in β-farnesene SOA suggests that their viscosity is higher than that of β-caryophyllene SOA. The higher abundance of aspherical particles at smaller sizes in β-farnesene SOA compared to β-caryophyllene SOA may be attributed to the acyclic structure and extra double bonds, which contribute to multifunctional oxidation products, and thus increase the overall particle viscosity of β-farnesene SOA. A detailed discussion of the SOA composition is provided in the offline analysis section.

The size-dependence of particle shape was additionally evaluated by looking at the trend in calculated particle densities/effective densities as a function of particle size. This approach supplements the qualitative assessment described in the previous paragraph. As the particle mobility diameter increased, there was a corresponding decrease in particle effective densities (Figure S3). Mathematically, this decrease means the vacuum aerodynamic diameter is becoming increasingly smaller than the mobility diameter at larger particle sizes, indicating that larger particles are more aspherical. The data were binned by spherical versus aspherical particles based on the broadness of the distribution and the density/effective density was calculated for each. The density of smaller spherical β-caryophyllene and β-farnesene SOA particles was calculated to be 1.17 ± 0.01 g/cm^3 and 1.20 ± 0.01 g/cm^3, respectively. However, the effective density of the larger, aspherical β-farnesene SOA particles with mobility diameter of 230 nm and d_{va} of 190 nm was 0.83 g/cm^3, which is significantly lower than the density of spherical β-farnesene SOA particles.

Particle Shape Evolution during Evaporation. For some of the SOA types (but not all), the shape of the particles in the evaporation chamber changed as the particles evaporated (Figure 3). This was evaluated by graphing the evolution of the vacuum aerodynamic diameter distributions (x-axis) over evaporation time (indicated with different colored lines). Recall, particle shape can be qualitatively characterized by the peak width and symmetry as described in the previous section. As the monoterpene SOA evaporated, the d_{va} distribution not only shifted to smaller values but also remained consistently narrow under both low and high RH (<10% and 75%, respectively) (Figure 3a and b show low RH conditions; Figure S3a and b show high RH conditions). This retention of the peak distribution over evaporation time indicates that the spherical shape of the particles was preserved throughout the evaporation process. The initial mobility size-selected particles that were used for the evaporation experiments were 165 nm for α-pinene SOA and 220 nm for β-ocimene SOA. These sizes were spherical when they were introduced to the evaporation chamber (see Figure 2 and associated text) and provided the required particle number concentrations (100−200 particles/cm^3) needed to minimize complicating particle interactions while also enabling the instrument to measure particle evaporation kinetics for many hours. The shape size-dependence of the sesquiterpene SOA introduced additional challenges in conducting and interpreting the evaporation experiments.

For the sesquiterpene SOA evaporation experiments, particle size selection targeted diameter ranges dominated by spherical particles to obtain narrow d_{va} distributions, thereby enabling the calculation of the volume fraction remaining (VFR). In the case of β-caryophyllene SOA, particles with d_m of 165 nm were spherical and had sufficient particle loadings to conduct the experiment. Throughout evaporation, β-caryophyllene SOA particles exhibited a consistently narrow d_{va} distribution under both low (RH < 10%) and high RH (75%) conditions indicating that the particle shape did not change over time (Figures 3c and S4c). In the case of β-farnesene SOA, particles with d_m of 140 nm represented a mixture of both aspherical and spherical shapes (Figure 3d) but also had high enough particle loadings to conduct the experiment. This mixture of particle shapes led to a broader, asymmetric d_{va} distribution; however, the peak maximum that corresponded to spherical particles remained clearly discernible in time-dependent d_{va} analysis (Figure 3d), allowing detailed study for the later evaporation kinetics. Notably, β-farnesene SOA particles underwent a rapid transition from aspherical to spherical shapes during evaporation in the dry evaporation chamber, coalescing within ∼ 30 min, as depicted in Figures 3d and S5. This shape transformation could be attributed to the thermodynamic drive toward minimizing surface energy, and the relaxation time scale can be used to estimate the SOA

https://doi.org/10.1021/acsestair.5c00226
ACS EST Air 2026, 3, 83−94

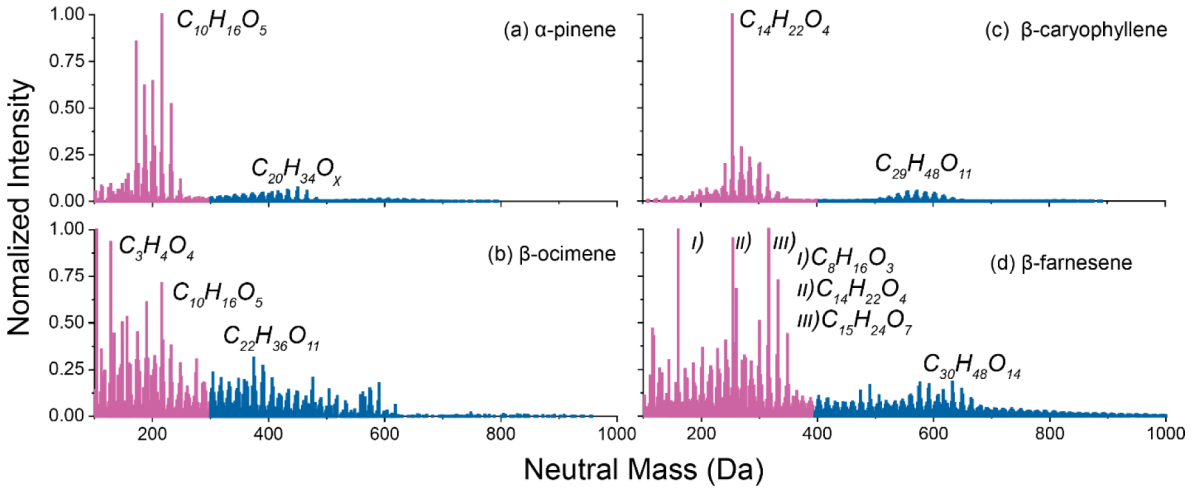

Figure 5. Nano-DESI mass spectra for SOA formed via OH photooxidation of a) α-pinene, b) β-ocimene, c) β-caryophyllene, and d) β-farnesene. Top monomer/dimer products are highlighted by red and blue based on their neutral mass. Note the difference of mass range for each SOA type.

material viscosity − an analysis that could not be conducted with the other SOA types since they were spherical throughout evaporation. Frenkel et al. described the relationship between the coalescence relaxation time (τ) and viscosity (η), $\tau = \frac{d\eta}{\sigma}$, where d represents the diameter of the particle (we used d_m in the calculation) and σ represents the surface tension.[56,57] Using the observed relaxation time of 15 min and a surface tension σ=0.023−0.045 N m^{-1},[58] we estimated the viscosity of β-farnesene SOA particles in the range of (1.4−2.8)×10^8 Pa s, which corresponds to a semisolid state at room temperature.

SOA Evaporation Kinetics. To further investigate differences in volatility and viscosity across SOA chemical systems, evaporation kinetics were measured under both dry and humid conditions. The evaporation kinetics show a two-stage process for all four SOA chemical systems (Figure 4), consistent with previous SOA evaporation kinetics measurements.[4,42] Initially, a rapid decrease in SOA volume occurs within the first 2−3 h, followed by a more gradual reduction of volume over a 24-h duration. During the initial rapid evaporation phase, the particles lose predominantly more volatile compounds,[59] leading to increased viscosity and decreased volatility of the residual particle, which contributes to slowing the evaporation rate.

We first discuss the particle evaporation kinetics under dry conditions (Figure 4). The evaporation kinetics of SOA particles from α-pinene, a cyclic monoterpene, exhibited a 54% decrease in volume within 200 min in the initial stage under dry conditions. This was followed by a slower rate of evaporation, ending with a 30% VFR at the final measurement (∼19 h), matching the previously reported VFR evolution for α-pinene under dry evaporation conditions.[42] For β-ocimene, an acyclic monoterpene, the SOA particles demonstrated a 37% loss in volume during the initial 200 min, with 49% of the original volume persisting after a 21-h period. This VFR was higher than that of α-pinene SOA, implying a significantly lower volatility of β-ocimene SOA compared to α-pinene SOA.

Cyclic sesquiterpene SOA, represented by β-caryophyllene, displayed a 36% volume reduction initially (∼200 min), with a subsequent VFR of approximately 54% after ∼ 18 h. Notably, the VFR of β-caryophyllene SOA was only ∼ 5% more than β-ocimene SOA, despite the former precursor having a larger molecular weight, which would typically be expected to result in lower volatility and higher viscosity SOA.[60] This highlights the importance of structural characteristics beyond molecular size alone for making predictions about SOA properties. The evaporation kinetics for β-farnesene SOA particles were characterized by an approximate 22% volume reduction within the first 200 min, concluding with a VFR of around 68% after 20 h, representing the least volatile SOA of all the chemical systems studied.

Under wet conditions (RH∼ 75%), we observed slightly higher evaporative losses compared to dry conditions across all SOA types (Figure 4). With increasing RH, particle viscosity decreases, and diffusivity within the bulk particle increases, facilitating greater evaporation for semivolatile organic compounds (SVOCs) that are trapped in highly viscous particles under dry conditions.[42,59] It is noteworthy that regardless of the SOA type, the differences in evaporation kinetics between wet and dry conditions were quite small, with the final VFR differing by only ∼ 10%.

Evaporation kinetics were used to fit a 7-bin VBS as an additional metric for evaluating SOA volatility. This analysis revealed that, within the monoterpene and sesquiterpene families, SOA from acyclic terpenes displayed a greater fraction in the extremely low volatility organic compound (ELVOC) and low volatility organic compound (LVOC) ranges, compared to SOA from cyclic terpene, which had a higher fractional contribution in the SVOC range (Figure S6; Tables S4 and S5). Recall, acyclic terpene SOA also had the highest viscosity based on the shape measurements and coalescence times. Because of the known anticorrelation between viscosity and volatility of SOA,[61] we expect the following order of viscosities for the SOA samples examined in this work: acyclic β-farnesene SOA > cyclic β-caryophyllene SOA > acyclic β-ocimene SOA > cyclic α-pinene SOA. This order is consistent with the observation of increased viscosity of SOA prepared from mixtures of VOCs which contain a higher proportion of sesquiterpenes.[33,34] The observed evaporation kinetics also indicated a shift in the condensed organic mass into lower volatility ELVOC/LVOC bins, slower modeled evaporation rates, and extended particle lifetimes relative to current modeling parametrizations based mainly on cyclic terpenes. Exploring SOA formed under wet versus dry conditions and subsequently evaporated at different RH conditions[42,62] is a

https://doi.org/10.1021/acsestair.5c00226
ACS EST Air 2026, 3, 83−94

natural follow-up for a future study but lies outside the scope of the present work.

Chemical Composition of SOA from HRMS. Figure 5 shows nano-DESI HRMS mass spectra of all SOA types and Figure S7 shows the carbon atom distribution of the observed compounds. The predominant monomer identified in α-pinene SOA was $C_{10}H_{16}O_5$, a formula commonly found in monoterpene SOA.[51,63,64] The previously proposed chemical pathway for $C_{10}H_{16}O_5$ includes RO_2 termination with HO_2, as discussed by McVay et al.[64] The most intense dimer signal in α-pinene SOA was associated with $C_{20}H_{34}O_x$ (x = 5−13), likely formed through the combination of two $C_{10}H_{17}O_x$ RO_2 species, which was thought to occur following OH addition and subsequent autoxidation.[65]

For β-ocimene, we observed $C_{10}H_{16}O_5$ as the most abundant monomer signal, which was the same for α-pinene SOA as they are isomeric compounds. The most intense peak detected for β-ocimene was attributed to the formula, $C_3H_4O_4$, suggesting extensive fragmentation during oxidation. The most intense oligomer peak was $C_{22}H_{36}O_{11}$, which was not found in α-pinene SOA. Gu et al. reported that β-ocimene oxidation in an oxidation flow reactor generates a substantial fraction of C_{11} products. Although C_{11} species were not the most intense peaks observed in the mass spectrum in our β-ocimene SOA, they were nevertheless detected (Figure S7b) and may serve as precursors to C_{22} species. These results indicate that, in contrast to α-pinene, β-ocimene follows distinct and more complex reaction pathways that require further investigation.

For β-caryophyllene SOA, the most pronounced peak was $C_{14}H_{22}O_4$ which is likely β-caryophyllinic acid, consistently observed in both field and laboratory measurements, and a key atmospheric tracer for β-caryophyllene.[66−69] The primary dimer identified in β-caryophyllene SOA was $C_{29}H_{48}O_{11}$, presumed to be formed from the reaction of C_{15} and C_{14} RO_2 species, which are two of the most abundant monomer families we observed.

The predominant peak detected in β-farnesene SOA was $C_{15}H_{24}O_7$, a highly oxygenated molecule that has been attributed to sesquiterpene oxidation products in both field studies and laboratory experiments.[70,71] Additionally, the most common dimer in β-farnesene SOA, $C_{30}H_{48}O_{14}$, may originate from a combination of two $C_{15}H_{24}O_x$ RO_2 species, but the detailed formation pathway remains unexplored.

Overall, the mass spectra of SOA derived from cyclic terpenes and acyclic terpenes looked qualitiatively different based on distribution of the peaks (Figure 5). Mass spectra of cyclic terpene-derived SOA showed a distinct separation between monomer and dimer regions, whereas SOA from acyclic terpenes displayed a broader distribution across the mass spectrum, featuring higher peak signal for both dimeric and fragmented compounds than their cyclic terpene counterparts (Figure 5 and Figure S7). The Shannon diversity index was calculated for each SOA type to compare formula product diversity to evaluate this distribution with a more quantitative approach, where a larger index value indicates a higher level of chemodiversity.[72] The acyclic terpene SOA exhibited higher diversity indices, with β-ocimene scoring 6.8 and β-farnesene scoring 6.7. In contrast, the cyclic terpene SOA had lower chemodiversity values, with α-pinene at 5.1 and β-caryophyllene at 5.7. These results are consistent with expected monomer reactivity, as acyclic terpenes contain more carbon−carbon double bonds than their cyclic analogs, providing more diverse reaction pathway and functional group addition. This therefore leads to increased chemical diversity of the oxidation products formed by both fragmentation and oligomerization reactions.[24,73] To further assess differences in SOA composition, hierarchical clustering was performed on the various samples according to their annotated organic molecular composition (Figure S8). This analysis evaluated whether the cyclic/acyclic nature or the monoterpene/sesquiterpene classification of precursor is a better predictor of the resulting SOA molecular composition. The clustering revealed that samples with higher similarity in their mass spectra were grouped together. Notably, β-ocimene and β-farnesene clustered closely, indicating a similar formula composition among the acyclic terpene-derived SOA. This result underscores the dominant role of precursor cyclicity in determining the trends in SOA composition. These compositional patterns and clustering results also highlight the strong influence of precursor cyclicity on SOA chemical diversity. The distinct mass-spectral signatures associated with cyclic and acyclic terpene-derived SOA could be leveraged in future modeling and source-apportionment efforts to interpret and constrain field measurements.

Utilizing chemical formulas acquired from nano-DESI-HRMS analysis, we applied the methodologies outlined by Li et al. and DeRieux et al. to predict the volatility and viscosity of individual SOA compounds, as well as the integrated SOA composition.[48,49,61] It is crucial to acknowledge, however, that this predictive approach utilizes the formula composition and does not incorporate considerations of chemical structure.[74] This approach also does not account for different relative ionization efficiencies of the SOA species. We acknowledge that offline HRMS analysis and usage of single polarity may limit the quantitative resolution of certain compounds, such as labile peroxides. However, the main purpose of this estimation is to provide a qualitative explanation for the observed evaporation kinetics in miniSPLAT experiments, and an important point of comparison for previously published papers that have also used this estimation technique for other SOA systems.[34,35,68]

Figure 6 illustrates the distribution of SOA products across volatility categories. The analysis indicates that for SOA derived from cyclic terpenes (α-pinene and β-caryophyllene), approximately 25% and 37% of their signals, respectively, fell within regions corresponding to ELVOCs and LVOCs. In contrast, SOA mass spectra from their acyclic terpene counterparts, β-ocimene and β-farnesene, showed a higher

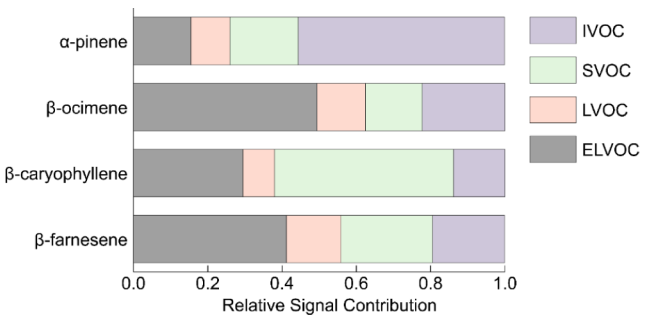

Figure 6. Relative contributions of each volatility category (ELVOCs ($C_0 < 3 \times 10^{-4}$ μg m^{-3}), LVOCs ($3 \times 10^{-4} < C_0 < 0.3$ μg m^{-3}), SVOCs ($0.3 < C_0 < 300$ μg m^{-3}), and IVOCs ($300 < C_0 < 3 \times 10^6$ μg m^{-3})) to the overall composition of SOA from OH oxidation of α-pinene, β-ocimene, β-caryophyllene, and β-farnesene.

https://doi.org/10.1021/acsestair.5c00226
ACS EST Air 2026, 3, 83−94

prevalence of signals attributed to ELVOCs and LVOCs, at 62% and 56%, respectively (Figure 6). Among the ELVOC and LVOC detected, in addition to the oligomeric compounds that may be enhanced in smog chamber experiments due to relatively high VOC concentrations and thus greater RO_2 availability, the SOA from acyclic terpenes also contained a larger fraction of ELVOC and LVOC present as monomeric/fragment ($C \leq 10$ for monoterpene and $C \leq 15$ for sesquiterpene SOA) components (0.8% for β-ocimene and 11% for β-farnesene) compared with SOA from cyclic terpenes (0.3% for α-pinene and 5% for β-caryophyllene). Because sesquiterpene precursors are less volatile than monoterpenes, their monomeric ELVOC/LVOC product fraction is correspondingly higher. The larger monomeric ELVOC/LVOC fraction in acyclic terpene SOA reflects their more efficient isomerization and autoxidation pathways compared to cyclic terpene, reducing volatility without changing the carbon skeleton, while fragmented ELVOC/LVOC indicate alkoxy radical pathways with C−C bond breakage. The average O:C ratios were quantified for different SOA types (Figure S9). The average O/C was similar for α-pinene (0.51), β-ocimene (0.53), and β-farnesene (0.51), but lower for β-caryophyllene (0.39).[75] A plausible explanation is that β-caryophyllene's complex double-ring structure may impose significant steric hindrance. This structure may reduce the molecule's accessibility to autoxidation pathways, instead favoring RO_2 pathways that produce less oxygenated and, therefore, more volatile products. The linear structure of acyclic terpenes results in less steric hindrance, which may facilitate pathways such as autoxidation, functionalization, and oligomerization which enhance the LVOC and ELVOC formation.

Using the observed chemical formulas, we predicted the viscosity of SOA from different types of VOCs under varying RH levels, as illustrated in Figure 7. At 0% RH, all SOA systems were predicted to be highly viscous.[76] With an increase in RH, the viscosity of all SOA systems decreased. However, the magnitude of this reduction varied depending on the chemical system. Specifically, within the monoterpene and sesquiterpene families, the calculation suggested that acyclic terpene SOA would remain viscous and may have a longer lifetime under a broader range of RH conditions in the lower atmosphere, from a compositional perspective. We emphasize that this analysis is not intended to predict SOA viscosity in a quantitative way, as absolute viscosity also depends on detailed molecular structure and interactions, but the relative ordering of SOA viscosity aligned well with our observations from evaporation kinetics experiments. Overall, the volatility and viscosity trends predicted from the mass spectra qualitatively matched the observations from evaporation kinetics: acyclic terpene SOA exhibited higher viscosity and lower volatility compared to SOA from the cyclic terpene analogs.

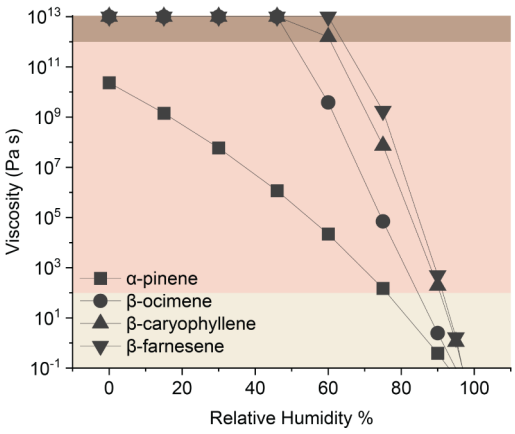

Figure 7. Predicted particle-phase viscosity of SOA derived from four different VOCs (α-pinene, β-ocimene, β-caryophyllene, and β-farnesene) as a function of water content. Viscosity predictions are based on the molecular formulas of assigned compounds. Shaded regions indicate viscosity benchmarks. From the darkest color, the viscosity ranges from solid, semisolid, to liquid.

CONCLUSIONS

By systematically comparing the particle shape and evaporation kinetics of SOA derived from OH oxidation of different terpenes, we have elucidated a clear trend in SOA viscosity as follows: α-pinene < β-ocimene < β-caryophyllene < β-farnesene, and a corresponding inverse trend in volatility: α-pinene > β-ocimene > β-caryophyllene > β-farnesene. In fact, the volatility and viscosity of β-ocimene SOA are comparable to those of β-caryophyllene SOA, suggesting that acyclic terpene can produce low-volatility products beyond the expectation based solely on their molecular weight. Further analysis of formula composition has shown SOA from OH oxidation of acyclic terpenes shows greater chemical diversity than that from cyclic terpenes, reflecting more complex oxidation pathways enabled by additional double bonds. For instance, OH can add at two different positions in α-pinene but at six in β-ocimene. The number of ways in which the resulting RO_2 can isomerize and RO radicals can fragment is also larger for acyclic compounds, leading to a greater diversity of products. The large portion of oligomers of acyclic terpene SOA contributes to their elevated viscosity and diminished volatility in comparison to cyclic terpene SOA.

These results have important implications. First, the physical properties of SOA from acyclic terpenes suggest that these compounds may influence aerosol lifetime, transport, and phase behavior in ways not fully captured by current models that focus on cyclic monoterpenes like α-pinene. For example, increased viscosity can slow down diffusion within particles, reduce rates of heterogeneous reactions, and inhibit mixing. Lower volatility can shift partitioning toward the particle phase and modify particle loading and their atmospheric lifetime. Additionally, as plants respond to environmental stressors, such as drought, heatwaves, and herbivore attacks, their emission profile is expected to change. This evolution in BVOC profiles could ultimately shift the physicochemical properties of atmospheric SOA. Together, we highlight a need to revisit how SOA precursors are represented in regional and global models. Without including more structurally diverse BVOC, current models may overlook pathways and feedback associated with other terpene structures, including those that may become more prominent in a changing environment which are necessary for estimation of SOA formation and mass loading. Incorporating a broader range of BVOC structures, especially under stress-driven emission scenarios, will improve predictions of aerosol formation and transformation, aerosol-cloud interactions, and the long-term atmospheric impacts of SOA. We suggest further study of acyclic terpenes through different SOA formation pathways with other oxidants, such as ozonolysis pathway, as well as their physicochemical properties and aerosol yield.

https://doi.org/10.1021/acsestair.5c00226
ACS EST Air 2026, 3, 83−94

■ ASSOCIATED CONTENT

Data Availability Statement

The data sets used to generate the figures and tables in this work are available in the Dryad Digital Repository at 10.5061/dryad.931zcrk0c.

Supporting Information

The Supporting Information is available free of charge at https://pubs.acs.org/doi/10.1021/acsestair.5c00226.

Tabular summary of experimental conditions, description of nano-DESI-HRMS and mass spectrometric data analysis, description of VBS fitting of evaporation data, description of volatility and viscosity estimation from the observed formula distribution, and additional figures and tables illustrating SOA particle properties, chemical composition, and volatility (PDF)

■ AUTHOR INFORMATION

Corresponding Author

Celia L. Faiola − *Department of Chemistry, University of California, Irvine, Irvine, California 92697, United States; Department of Ecology and Evolutionary Biology, University of California Irvine, Irvine, California 92697, United States;* orcid.org/0000-0002-4987-023X; Email: cfaiola@uci.edu

Authors

Sijia Liu − *Department of Chemistry, University of California, Irvine, Irvine, California 92697, United States; Environmental Molecular Sciences Laboratory, Pacific Northwest National Laboratory, Richland, Washington 99354, United States;* orcid.org/0000-0002-6958-2868

Claire E. Moffett − *Atmospheric, Climate, & Earth Sciences Division, Pacific Northwest National Laboratory, Richland, Washington 99354, United States*

Gregory Vandergrift − *Environmental Molecular Sciences Laboratory, Pacific Northwest National Laboratory, Richland, Washington 99354, United States;* orcid.org/0000-0002-8962-9897

Manish Shrivastava − *Environmental Molecular Sciences Laboratory, Pacific Northwest National Laboratory, Richland, Washington 99354, United States;* orcid.org/0000-0002-9053-2400

Zezhen Cheng − *Environmental Molecular Sciences Laboratory, Pacific Northwest National Laboratory, Richland, Washington 99354, United States;* orcid.org/0000-0001-6320-4519

Swarup China − *Environmental Molecular Sciences Laboratory, Pacific Northwest National Laboratory, Richland, Washington 99354, United States;* orcid.org/0000-0001-7670-335X

Sergey A. Nizkorodov − *Department of Chemistry, University of California, Irvine, Irvine, California 92697, United States;* orcid.org/0000-0003-0891-0052

Alla Zelenyuk − *Atmospheric, Climate, & Earth Sciences Division, Pacific Northwest National Laboratory, Richland, Washington 99354, United States;* orcid.org/0000-0002-0674-0910

Complete contact information is available at: https://pubs.acs.org/10.1021/acsestair.5c00226

Author Contributions

C.L.F. and S.A.N. conceived the project and contributed to experimental design and interpretation. S.L. designed and conducted the experiments, analyzed the data, interpreted the results, drafted the manuscript, and generated the figures. C.E.M. and A.Z. performed miniSPLAT measurements and data analysis. S.L. and G.V. conducted and interpreted the nano-DESI-HRMS measurements. Z.C. and S.C. assisted with sample collection and interpretation. M.S. and S.L. performed the VBS fitting for evaporation kinetics. All authors discussed the results and contributed to manuscript revisions.

Funding

This research was supported by NSF AGS-2334731 *C.L.F. was supported by NSF AGS-2414615. C.M., M.S., and A.Z. were supported by the Atmospheric System Research (ASR) program as part of the U.S. Department of Energy Office of Biological and Environmental Research under PNNL ICLASS project KP1701010/57131. Pacific Northwest National Laboratory is operated by DOE by the Battelle Memorial Institute under Contract DE-A06−76RLO1830. Additionally, S.L thanks the Department of Chemistry, University of California, Irvine, for support with the Rowland Graduate Research Fellowship.

Notes

The authors declare no competing financial interest.

■ REFERENCES

(1) Srivastava, D.; Vu, T. V.; Tong, S.; Shi, Z.; Harrison, R. M. Formation of Secondary Organic Aerosols from Anthropogenic Precursors in Laboratory Studies. *Npj Clim. Atmos. Sci.* **2022**, *5* (1), 22.

(2) Pye, H. O. T.; Ward-Caviness, C. K.; Murphy, B. N.; Appel, K. W.; Seltzer, K. M. Secondary Organic Aerosol Association with Cardiorespiratory Disease Mortality in the United States. *Nat. Commun.* **2021**, *12* (1), 7215.

(3) Zhu, J.; Penner, J. E.; Lin, G.; Zhou, C.; Xu, L.; Zhuang, B. Mechanism of SOA Formation Determines Magnitude of Radiative Effects. *Proc. Natl. Acad. Sci. U. S. A.* **2017**, *114* (48), 12685−12690.

(4) Vaden, T. D.; Imre, D.; Beránek, J.; Shrivastava, M.; Zelenyuk, A. Evaporation Kinetics and Phase of Laboratory and Ambient Secondary Organic Aerosol. *Proc. Natl. Acad. Sci. U. S. A.* **2011**, *108* (6), 2190−2195.

(5) Vaden, T. D.; Song, C.; Zaveri, R. A.; Imre, D.; Zelenyuk, A. Morphology of Mixed Primary and Secondary Organic Particles and the Adsorption of Spectator Organic Gases during Aerosol Formation. *Proc. Natl. Acad. Sci. U. S. A.* **2010**, *107* (15), 6658−6663.

(6) Ignatius, K.; Kristensen, T. B.; Järvinen, E.; Nichman, L.; Fuchs, C.; Gordon, H.; Herenz, P.; Hoyle, C. R.; Duplissy, J.; Garimella, S.; Dias, A.; Frege, C.; Höppel, N.; Tröstl, J.; Wagner, R.; Yan, C.; Amorim, A.; Baltensperger, U.; Curtius, J.; Donahue, N. M.; Gallagher, M. W.; Kirkby, J.; Kulmala, M.; Möhler, O.; Saathoff, H.; Schnaiter, M.; Tomé, A.; Virtanen, A.; Worsnop, D.; Stratmann, F. Heterogeneous Ice Nucleation of Viscous Secondary Organic Aerosol Produced from Ozonolysis of α-Pinene. *Atmos. Chem. Phys.* **2016**, *16* (10), 6495−6509.

(7) Lignell, H.; Hinks, M. L.; Nizkorodov, S. A. Exploring Matrix Effects on Photochemistry of Organic Aerosols. *Proc. Natl. Acad. Sci. U. S. A.* **2014**, *111* (38), 13780−13785.

(8) Guenther, A.; Zimmerman, P.; Wildermuth, M. Natural Volatile Organic Compound Emission Rate Estimates for U.S. Woodland Landscapes. *Atmos. Environ.* **1994**, *28* (6), 1197−1210.

(9) Guenther, A.; Hewitt, C. N.; Erickson, D.; Fall, R.; Geron, C.; Graedel, T.; Harley, P.; Klinger, L.; Lerdau, M.; Mckay, W. A.; Pierce, T.; Scholes, B.; Steinbrecher, R.; Tallamraju, R.; Taylor, J.; Zimmerman, P. A Global Model of Natural Volatile Organic

Compound Emissions. *J. Geophys. Res. :Atmos.* **1995**, *100* (D5), 8873−8892.
(10) Guenther, A. B.; Jiang, X.; Heald, C. L.; Sakulyanontvittaya, T.; Duhl, T.; Emmons, L. K.; Wang, X. The Model of Emissions of Gases and Aerosols from Nature Version 2.1 (MEGAN2.1): An Extended and Updated Framework for Modeling Biogenic Emissions. *Geosci. Model Dev.* **2012**, *5* (6), 1471−1492.
(11) Arimura, G.; Kost, C.; Boland, W. H.-I. Indirect Plant Defences. *Biochim. Biophys. Acta, Mol. Cell Biol. Lipids* **2005**, *1734* (2), 91−111.
(12) Arimura, G.; Ozawa, R.; Shimoda, T.; Nishioka, T.; Boland, W.; Takabayashi, J. Herbivory-Induced Volatiles Elicit Defence Genes in Lima Bean Leaves. *Nature* **2000**, *406* (6795), 512−515.
(13) Blande, J. D.; Tiiva, P.; Oksanen, E.; Holopainen, J. K. Emission of Herbivore-Induced Volatile Terpenoids from Two Hybrid Aspen (Populus Tremula × tremuloides) Clones under Ambient and Elevated Ozone Concentrations in the Field. *Glob. Change Biol.* **2007**, *13* (12), 2538−2550.
(14) Moura, B. B.; Bolsoni, V. P.; de Paula, M. D.; Dias, G. M.; de Souza, S. R. Ozone Impact on Emission of Biogenic Volatile Organic Compounds in Three Tropical Tree Species From the Atlantic Forest Remnants in Southeast Brazil. *Front. Plant Sci.* **2022**, *13*, 879039.
(15) Šimpraga, M.; Ghimire, R. P.; Van Der Straeten, D.; Blande, J. D.; Kasurinen, A.; Sorvari, J.; Holopainen, T.; Adriaenssens, S.; Holopainen, J. K.; Kivimäenpää, M. Unravelling the Functions of Biogenic Volatiles in Boreal and Temperate Forest Ecosystems. *Eur. J. For. Res.* **2019**, *138* (5), 763−787.
(16) Feldner, J.; Ramacher, M. O. P.; Karl, M.; Quante, M.; Luttkus, M. L. Analysis of the Effect of Abiotic Stressors on BVOC Emissions from Urban Green Infrastructure in Northern Germany. *Environ. Sci.: Atmos.* **2022**, *2* (5), 1132−1151.
(17) Eckardt, N. A.; Cutler, S.; Juenger, T. E.; Marshall-Colon, A.; Udvardi, M.; Verslues, P. E. Focus on Climate Change and Plant Abiotic Stress Biology. *Plant Cell* **2023**, *35* (1), 1.
(18) Ghimire, R. P.; Silfver, T.; Myller, K.; Oksanen, E.; Holopainen, J. K.; Mikola, J. BVOC Emissions From a Subarctic Ecosystem, as Controlled by Insect Herbivore Pressure and Temperature. *Ecosystems* **2022**, *25* (4), 872−891.
(19) Boncan, D. A. T.; Tsang, S. S. K.; Li, C.; Lee, I. H. T.; Lam, H.-M.; Chan, T.-F.; Hui, J. H. L. Terpenes and Terpenoids in Plants: Interactions with Environment and Insects. *Int. J. Mol. Sci.* **2020**, *21* (19), 7382.
(20) Fitzky, A. C.; Kaser, L.; Peron, A.; Karl, T.; Graus, M.; Tholen, D.; Halbwirth, H.; Trimmel, H.; Pesendorfer, M.; Rewald, B.; Sandén, H. S. Same, but Different: Drought and Salinity Affect BVOC Emission Rate and Alter Blend Composition of Urban Trees. *Urban For. Urban Greening* **2023**, *80*, 127842.
(21) Ghirardo, A.; Xie, J.; Zheng, X.; Wang, Y.; Grote, R.; Block, K.; Wildt, J.; Mentel, T.; Kiendler-Scharr, A.; Hallquist, M.; Butterbach-Bahl, K.; Schnitzler, J. P. Urban Stress-Induced Biogenic VOC Emissions and SOA-Forming Potentials in Beijing. *Atmos. Chem. Phys.* **2016**, *16* (5), 2901−2920.
(22) Mentel, T. F.; Kleist, E.; Andres, S.; Dal Maso, M.; Hohaus, T.; Kiendler-Scharr, A.; Rudich, Y.; Springer, M.; Tillmann, R.; Uerlings, R.; Wahner, A.; Wildt, J. Secondary Aerosol Formation from Stress-Induced Biogenic Emissions and Possible Climate Feedbacks. *Atmos. Chem. Phys.* **2013**, *13* (17), 8755−8770.
(23) Niinemets, Ü. Mild versus Severe Stress and BVOCs: Thresholds, Priming and Consequences. *Trends Plant Sci.* **2010**, *15* (3), 145−153.
(24) Khalaj, F.; Rivas-Ubach, A.; Anderton, C. R.; China, S.; Mooney, K.; Faiola, C. L. Acyclic Terpenes Reduce Secondary Organic Aerosol Formation from Emissions of a Riparian Shrub. *ACS Earth Space Chem.* **2021**, *5* (5), 1242−1253.
(25) Niinemets, Ü.; Kännaste, A.; Copolovici, L. Quantitative Patterns between Plant Volatile Emissions Induced by Biotic Stresses and the Degree of Damage. *Front. Plant Sci.* **2013**, *4*, 49750.
(26) Jardine, A. B.; Jardine, K. J.; Fuentes, J. D.; Martin, S. T.; Martins, G.; Durgante, F.; Carneiro, V.; Higuchi, N.; Manzi, A. O.; Chambers, J. Q. Highly Reactive Light-Dependent Monoterpenes in the Amazon. *Geophys. Res. Lett.* **2015**, *42* (5), 1576−1583.
(27) Shaw, J. T.; Lidster, R. T.; Cryer, D. R.; Ramirez, N.; Whiting, F. C.; Boustead, G. A.; Whalley, L. K.; Ingham, T.; Rickard, A. R.; Dunmore, R. E.; Heard, D. E.; Lewis, A. C.; Carpenter, L. J.; Hamilton, J. F.; Dillon, T. J. A. S.-C. Multivariate Method for the Determination of Gas-Phase Rate Coefficients, Applied to Reactions of Atmospheric VOCs and the Hydroxyl Radical. *Atmos. Chem. Phys.* **2018**, *18* (6), 4039−4054.
(28) Atkinson, R. Kinetics of the Gas-Phase Reactions of OH Radicals with Alkanes and Cycloalkanes. *Atmos. Chem. Phys.* **2003**, *3* (6), 2233−2307.
(29) Atkinson, R.; Baulch, D. L.; Cox, R. A.; Crowley, J. N.; Hampson, R. F.; Hynes, R. G.; Jenkin, M. E.; Rossi, M. J.; Troe, J. IUPAC Subcommittee. Evaluated Kinetic and Photochemical Data for Atmospheric Chemistry: Volume II − Gas Phase Reactions of Organic Species. *Atmos. Chem. Phys.* **2006**, *6* (11), 3625−4055.
(30) Faiola, C. L.; Pullinen, I.; Buchholz, A.; Khalaj, F.; Ylisirniö, A.; Kari, E.; Miettinen, P.; Holopainen, J. K.; Kivimäenpää, M.; Schobesberger, S.; Yli-Juuti, T.; Virtanen, A. Secondary Organic Aerosol Formation from Healthy and Aphid-Stressed Scots Pine Emissions. *ACS Earth Space Chem.* **2019**, *3* (9), 1756−1772.
(31) Ylisirniö, A.; Buchholz, A.; Mohr, C.; Li, Z.; Barreira, L.; Lambe, A.; Faiola, C.; Kari, E.; Yli-Juuti, T.; Nizkorodov, S. A.; Worsnop, D. R.; Virtanen, A.; Schobesberger, S. Composition and Volatility of Secondary Organic Aerosol (SOA) Formed from Oxidation of Real Tree Emissions Compared to Simplified Volatile Organic Compound (VOC) Systems. *Atmos. Chem. Phys.* **2020**, *20* (9), 5629−5644.
(32) Morales, A. C.; Jayarathne, T.; Slade, J. H.; Laskin, A.; Shepson, P. B. The Production and Hydrolysis of Organic Nitrates from OH Radical Oxidation of β-Ocimene. *Atmos. Chem. Phys.* **2021**, *21* (1), 129−145.
(33) Smith, N. R.; Crescenzo, G. V.; Huang, Y.; Hettiyadura, A. P. S.; Siemens, K.; Li, Y.; Faiola, C. L.; Laskin, A.; Shiraiwa, M.; Bertram, A. K.; Nizkorodov, S. A. Viscosity and Liquid−Liquid Phase Separation in Healthy and Stressed Plant SOA. *Environ. Sci. Atmos.* **2021**, *1* (3), 140−153.
(34) Smith, N. R.; Crescenzo, G. V.; Bertram, A. K.; Nizkorodov, S. A.; Faiola, C. L. Insect Infestation Increases Viscosity of Biogenic Secondary Organic Aerosol. *ACS Earth Space Chem.* **2023**, *7* (5), 1060−1071.
(35) Liu, S.; Galeazzo, T.; Valorso, R.; Shiraiwa, M.; Faiola, C. L.; Nizkorodov, S. A. Secondary Organic Aerosol from OH-Initiated Oxidation of Mixtures of d-Limonene and β-Myrcene. *Environ. Sci. Technol.* **2024**, *58* (30), 13391−13401.
(36) Barreira, L. M. F.; Ylisirniö, A.; Pullinen, I.; Buchholz, A.; Li, Z.; Lipp, H.; Junninen, H.; Hõrrak, U.; Noe, S. M.; Krasnova, A.; Krasnov, D.; Kask, K.; Talts, E.; Niinemets, Ü.; Ruiz-Jimenez, J.; Schobesberger, S. The Importance of Sesquiterpene Oxidation Products for Secondary Organic Aerosol Formation in a Springtime Hemiboreal Forest. *Atmos. Chem. Phys.* **2021**, *21* (15), 11781−11800.
(37) Helmig, D.; Ortega, J.; Duhl, T.; Tanner, D.; Guenther, A.; Harley, P.; Wiedinmyer, C.; Milford, J.; Sakulyanontvittaya, T. Sesquiterpene Emissions from Pine Trees − Identifications, Emission Rates and Flux Estimates for the Contiguous United States. *Environ. Sci. Technol.* **2007**, *41* (5), 1545−1553.
(38) Zelenyuk, A.; Yang, J.; Choi, E.; Imre, D. SPLAT II: An Aircraft Compatible, Ultra-Sensitive, High Precision Instrument for In-Situ Characterization of the Size and Composition of Fine and Ultrafine Particles. *Aerosol Sci. Technol.* **2009**, *43* (5), 411−424.
(39) Zelenyuk, A.; Yang, J.; Song, C.; Zaveri, R. A.; Imre, D. "Depth-Profiling" and Quantitative Characterization of the Size, Composition, Shape, Density, and Morphology of Fine Particles with SPLAT, a Single-Particle Mass Spectrometer. *J. Phys. Chem. A* **2008**, *112* (4), 669−677.
(40) Zelenyuk, A.; Imre, D.; Wilson, J.; Zhang, Z.; Wang, J.; Mueller, K. Airborne Single Particle Mass Spectrometers (SPLAT II & miniSPLAT) and New Software for Data Visualization and Analysis in

https://doi.org/10.1021/acsestair.5c00226
ACS EST Air 2026, 3, 83−94

a Geo-Spatial Context. *J. Am. Soc. Mass Spectrom.* **2015**, *26* (2), 257−270.
(41) Hinks, M. L.; Montoya-Aguilera, J.; Ellison, L.; Lin, P.; Laskin, A.; Laskin, J.; Shiraiwa, M.; Dabdub, D.; Nizkorodov, S. A. Effect of Relative Humidity on the Composition of Secondary Organic Aerosol from the Oxidation of Toluene. *Atmos. Chem. Phys.* **2018**, *18* (3), 1643−1652.
(42) Wilson, J.; Imre, D.; Beránek, J.; Shrivastava, M.; Zelenyuk, A. Evaporation Kinetics of Laboratory-Generated Secondary Organic Aerosols at Elevated Relative Humidity. *Environ. Sci. Technol.* **2015**, *49* (1), 243−249.
(43) Shrivastava, M.; Cappa, C. D.; Fan, J.; Goldstein, A. H.; Guenther, A. B.; Jimenez, J. L.; Kuang, C.; Laskin, A.; Martin, S. T.; Ng, N. L.; Petaja, T.; Pierce, J. R.; Rasch, P. J.; Roldin, P.; Seinfeld, J. H.; Shilling, J.; Smith, J. N.; Thornton, J. A.; Volkamer, R.; Wang, J.; Worsnop, D. R.; Zaveri, R. A.; Zelenyuk, A.; Zhang, Q. Recent Advances in Understanding Secondary Organic Aerosol: Implications for Global Climate Forcing. *Rev. Geophys.* **2017**, *55* (2), 509−559.
(44) Resch, J.; Wolfer, K.; Barth, A.; Kalberer, M. Effects of Storage Conditions on the Molecular-Level Composition of Organic Aerosol Particles. *Atmos. Chem. Phys.* **2023**, *23* (16), 9161−9171.
(45) Vandergrift, G. W.; Dexheimer, D. N.; Zhang, D.; Cheng, Z.; Lata, N. N.; Rogers, M. M.; Shrivastava, M.; Zhang, J.; Gaudet, B. J.; Mei, F.; China, S. Tethered Balloon System and High-Resolution Mass Spectrometry Reveal Increased Organonitrates Aloft Compared to the Ground Level. *Environ. Sci. Technol.* **2024**, *58* (23), 10060−10071.
(46) Vandergrift, G. W.; Shawon, A. S. M.; Dexheimer, D. N.; Zawadowicz, M. A.; Mei, F.; China, S. Molecular Characterization of Organosulfate-Dominated Aerosols over Agricultural Fields from the Southern Great Plains by High-Resolution Mass Spectrometry. *ACS Earth Space Chem.* **2022**, *6* (7), 1733−1741.
(47) Schum, S. K.; Brown, L. E.; Mazzoleni, L. R. MFAssignR: Molecular Formula Assignment Software for Ultrahigh Resolution Mass Spectrometry Analysis of Environmental Complex Mixtures. *Environ. Res.* **2020**, *191*, 110114.
(48) Li, Y.; Pöschl, U.; Shiraiwa, M. Molecular Corridors and Parameterizations of Volatility in the Chemical Evolution of Organic Aerosols. *Atmos. Chem. Phys.* **2016**, *16* (5), 3327−3344.
(49) DeRieux, W. S. W.; Li, Y.; Lin, P.; Laskin, J.; Laskin, A.; Bertram, A. K.; Nizkorodov, S. A.; Shiraiwa, M. Predicting the Glass Transition Temperature and Viscosity of Secondary Organic Material Using Molecular Composition. *Atmos. Chem. Phys.* **2018**, *18* (9), 6331−6351.
(50) Zelenyuk, A.; Yang, J.; Song, C.; Zaveri, R. A.; Imre, D. A New Real-Time Method for Determining Particles' Sphericity and Density: Application to Secondary Organic Aerosol Formed by Ozonolysis of α-Pinene. *Environ. Sci. Technol.* **2008**, *42* (21), 8033−8038.
(51) Shilling, J. E.; Chen, Q.; King, S. M.; Rosenoern, T.; Kroll, J. H.; Worsnop, D. R.; DeCarlo, P. F.; Aiken, A. C.; Sueper, D.; Jimenez, J. L.; Martin, S. T. Loading-Dependent Elemental Composition of α-Pinene SOA Particles. *Atmos. Chem. Phys.* **2009**, *9* (3), 771−782.
(52) Bell, D. M.; Imre, D.; Martin, S. T.; Zelenyuk, A. The Properties and Behavior of α-Pinene Secondary Organic Aerosol Particles Exposed to Ammonia under Dry Conditions. *Phys. Chem. Chem. Phys.* **2017**, *19* (9), 6497−6507.
(53) Rothfuss, N. E.; Petters, M. D. Coalescence-Based Assessment of Aerosol Phase State Using Dimers Prepared through a Dual-Differential Mobility Analyzer Technique. *Aerosol Sci. Technol.* **2016**, *50* (12), 1294−1305.
(54) Zhang, Y.; Sanchez, M. S.; Douet, C.; Wang, Y.; Bateman, A. P.; Gong, Z.; Kuwata, M.; Renbaum-Wolff, L.; Sato, B. B.; Liu, P. F.; Bertram, A. K.; Geiger, F. M.; Martin, S. T. Changing Shapes and Implied Viscosities of Suspended Submicron Particles. *Atmos. Chem. Phys.* **2015**, *15* (14), 7819−7829.
(55) Järvinen, E.; Ignatius, K.; Nichman, L.; Kristensen, T. B.; Fuchs, C.; Hoyle, C. R.; Höppel, N.; Corbin, J. C.; Craven, J.; Duplissy, J.; Ehrhart, S.; El Haddad, I.; Frege, C.; Gordon, H.; Jokinen, T.; Kallinger, P.; Kirkby, J.; Kiselev, A.; Naumann, K.-H.; Petäjä, T.; Pinterich, T.; Prevot, A. S. H.; Saathoff, H.; Schiebel, T.; Sengupta, K.; Simon, M.; Slowik, J. G.; Tröstl, J.; Virtanen, A.; Vochezer, P.; Vogt, S.; Wagner, A. C.; Wagner, R.; Williamson, C.; Winkler, P. M.; Yan, C.; Baltensperger, U.; Donahue, N. M.; Flagan, R. C.; Gallagher, M.; Hansel, A.; Kulmala, M.; Stratmann, F.; Worsnop, D. R.; Möhler, O.; Leisner, T.; Schnaiter, M. Observation of Viscosity Transition in α-Pinene Secondary Organic Aerosol. *Atmos. Chem. Phys.* **2016**, *16* (7), 4423−4438.
(56) Frenkel, J. Viscous Flow Of Crystalline Bodies Under The Action Of Surface Tension. *J. Phys.* **1945**, *9*, 385.
(57) Pajunoja, A.; Malila, J.; Hao, L.; Joutsensaari, J.; Lehtinen, K. E.; Virtanen, A. Estimating the Viscosity Range of SOA Particles Based on Their Coalescence Time. *Aerosol Sci. Technol.* **2014**, *48* (2), i−iv.
(58) Kiland, K. J.; Marroquin, K. L.; Smith, N. R.; Xu, S.; Nizkorodov, S. A.; Bertram, A. K. A New Hot-Stage Microscopy Technique for Measuring Temperature-Dependent Viscosities of Aerosol Particles and Its Application to Farnesene Secondary Organic Aerosol. *Atmos. Meas. Technol.* **2022**, *15* (19), 5545−5561.
(59) Yli-Juuti, T.; Pajunoja, A.; Tikkanen, O.-P.; Buchholz, A.; Faiola, C.; Väisänen, O.; Hao, L.; Kari, E.; Peräkylä, O.; Garmash, O.; Shiraiwa, M.; Ehn, M.; Lehtinen, K.; Virtanen, A. Factors Controlling the Evaporation of Secondary Organic Aerosol from α-Pinene Ozonolysis. *Geophys. Res. Lett.* **2017**, *44* (5), 2562−2570.
(60) Li, Z.; Buchholz, A.; Ylisirniö, A.; Barreira, L.; Hao, L.; Schobesberger, S.; Yli-Juuti, T.; Virtanen, A. Evolution of Volatility and Composition in Sesquiterpene-Mixed and α-Pinene Secondary Organic Aerosol Particles during Isothermal Evaporation. *Atmos. Chem. Phys.* **2021**, *21* (24), 18283−18302.
(61) Li, Y.; Day, D. A.; Stark, H.; Jimenez, J. L.; Shiraiwa, M. Predictions of the Glass Transition Temperature and Viscosity of Organic Aerosols from Volatility Distributions. *Atmos. Chem. Phys.* **2020**, *20* (13), 8103−8122.
(62) Zaveri, R. A.; Shilling, J. E.; Zelenyuk, A.; Zawadowicz, M. A.; Suski, K.; China, S.; Bell, D. M.; Veghte, D.; Laskin, A. Particle-Phase Diffusion Modulates Partitioning Of Semivolatile Organic Compounds To Aged Secondary Organic Aerosol. *Environ. Sci. Technol.* **2020**, *54*, 2595−2605.
(63) Hammes, J.; Lutz, A.; Mentel, T.; Faxon, C.; Hallquist, M. Carboxylic Acids from Limonene Oxidation by Ozone and Hydroxyl Radicals: Insights into Mechanisms Derived Using a FIGAERO-CIMS. *Atmos. Chem. Phys.* **2019**, *19* (20), 13037−13052.
(64) McVay, R. C.; Zhang, X.; Aumont, B.; Valorso, R.; Camredon, M.; La, Y. S.; Wennberg, P. O.; Seinfeld, J. H. SOA Formation from the Photooxidation of α-Pinene: Systematic Exploration of the Simulation of Chamber Data. *Atmos. Chem. Phys.* **2016**, *16* (5), 2785−2802.
(65) Baker, Y.; Kang, S.; Wang, H.; Wu, R.; Xu, J.; Zanders, A.; He, Q.; Hohaus, T.; Ziehm, T.; Geretti, V.; et al. Impact of HO_2/RO_2 Ratio on Highly Oxygenated α-Pinene Photooxidation Products and Secondary Organic Aerosol Formation Potential; preprint; Gases/Laboratory Studies/Troposphere/Chemistry. *Atmos. Chem. Phys.* **2023**, *24*, 4789−4807.
(66) Jaoui, M.; Lewandowski, M.; Kleindienst, T. E.; Offenberg, J. H.; Edney, E. O. β-Caryophyllinic Acid: An Atmospheric Tracer for β-Caryophyllene Secondary Organic Aerosol. *Geophys. Res. Lett.* **2007**, *34*(5). .
(67) Li, Y. J.; Chen, Q.; Guzman, M. I.; Chan, C. K.; Martin, S. T. Second-Generation Products Contribute Substantially to the Particle-Phase Organic Material Produced by β-Caryophyllene Ozonolysis. *Atmos. Chem. Phys.* **2011**, *11* (1), 121−132.
(68) Maclean, A. M.; Smith, N. R.; Li, Y.; Huang, Y.; Hettiyadura, A. P. S.; Crescenzo, G. V.; Shiraiwa, M.; Laskin, A.; Nizkorodov, S. A.; Bertram, A. K. Humidity-Dependent Viscosity of Secondary Organic Aerosol from Ozonolysis of β-Caryophyllene: Measurements, Predictions, and Implications. *ACS Earth Space Chem.* **2021**, *5* (2), 305−318.
(69) Gao, L.; Song, J.; Mohr, C.; Huang, W.; Vallon, M.; Jiang, F.; Leisner, T.; Saathoff, H. Kinetics, SOA Yields and Chemical

https://doi.org/10.1021/acsestair.5c00226
ACS EST Air 2026, 3, 83−94

Composition of Secondary Organic Aerosol from β-Caryophyllene Ozonolysis with and without Nitrogen Oxides between 213 and 313 K; preprint; Aerosols/Laboratory studies/Troposphere/Chemistry (Chemical Composition And Reactions). *Atmos. Chem. Phys.* **2022**, *22*, 6001−6020.
(70) Klodt, A. L.; Romonosky, D. E.; Lin, P.; Laskin, J.; Laskin, A.; Nizkorodov, S. A. Aqueous Photochemistry of Secondary Organic Aerosol of α-Pinene and α-Humulene in the Presence of Hydrogen Peroxide or Inorganic Salts. *ACS Earth Space Chem.* **2019**, *3* (12), 2736−2746.
(71) Bianchi, F.; Kurtén, T.; Riva, M.; Mohr, C.; Rissanen, M. P.; Roldin, P.; Berndt, T.; Crounse, J. D.; Wennberg, P. O.; Mentel, T. F.; Wildt, J.; Junninen, H.; Jokinen, T.; Kulmala, M.; Worsnop, D. R.; Thornton, J. A.; Donahue, N.; Kjaergaard, H. G.; Ehn, M. Highly Oxygenated Organic Molecules (HOM) from Gas-Phase Autoxidation Involving Peroxy Radicals: A Key Contributor to Atmospheric Aerosol. *Chem. Rev.* **2019**, *119* (6), 3472−3509.
(72) Shannon, C. E. A Mathematical Theory of Communication. *Bell Syst. Technol. J.* **1948**, *27* (3), 379−423.
(73) Takeuchi, M.; Berkemeier, T.; Eris, G.; Ng, N. L. Non-Linear Effects of Secondary Organic Aerosol Formation and Properties in Multi-Precursor Systems. *Nat. Commun.* **2022**, *13* (1), 1−13.
(74) Kenseth, C. M.; Hafeman, N. J.; Huang, Y.; Dalleska, N. F.; Stoltz, B. M.; Seinfeld, J. H. Synthesis of Carboxylic Acid and Dimer Ester Surrogates to Constrain the Abundance and Distribution of Molecular Products in α-Pinene and β-Pinene Secondary Organic Aerosol. *Environ. Sci. Technol.* **2020**, *54*, 12829−12839.
(75) Wang, J.; Shilling, J. E.; Liu, J.; Zelenyuk, A.; Bell, D. M.; Petters, M. D.; Thalman, R.; Mei, F.; Zaveri, R. A.; Zheng, G. Cloud Droplet Activation of Secondary Organic Aerosol Is Mainly Controlled by Molecular Weight, Not Water Solubility. *Atmos. Chem. Phys.* **2019**, *19* (2), 941−954.
(76) Koop, T.; Bookhold, J.; Shiraiwa, M.; Pöschl, U. Glass Transition and Phase State of Organic Compounds: Dependency on Molecular Properties and Implications for Secondary Organic Aerosols in the Atmosphere. *Phys. Chem. Chem. Phys.* **2011**, *13* (43), 19238−19255.

https://doi.org/10.1021/acsestair.5c00226
ACS EST Air 2026, 3, 83−94